AD-A275 112

TATION PAGE

Form Approved
OMB No 0704 0188

1 AGENCY USE ONLY (Leave blank)	2 REPORT DATE December 1993	3 REPORT TYPE AND DATES COVERED Professional Paper

4 TITLE AND SUBTITLE

VLF SOURCE LOCALIZATION WITH A FREELY DRIFTING ACOUSTIC SENSOR ARRAY

5 FUNDING NUMBERS

PR: SUB8
PE: 0602314N
WN: DN308105

6 AUTHOR(S)

G. Chen and W. Hodgkiss

7 PERFORMING ORGANIZATION NAME(S) AND ADDRESS(ES)

Naval Command, Control and Ocean Surveillance Center (NCCOSC)
RDT&E Division
San Diego, CA 92152–5001

8 PERFORMING ORGANIZATION REPORT NUMBER

9 SPONSORING/MONITORING AGENCY NAME(S) AND ADDRESS(ES)

Naval Command, Control and Ocean Surveillance Center (NCCOSC)
RDT&E Division
San Diego, CA 92152–5001

10 SPONSORING/MONITORING AGENCY REPORT NUMBER

11 SUPPLEMENTARY NOTES

12a DISTRIBUTION/AVAILABILITY STATEMENT

Approved for public release; distribution is unlimited.

94-01572

13 ABSTRACT (Maximum 200 words)

This paper describes the source localization and tracking capability of a freely drifting volumetric array with matched-field processing (MFP) using experimental data.

Published in *IEEE Journal of Oceanic Engineering*, July 1993, pp. 209–223.

Accesion For		
NTIS	CRA&I	☑
DTIC	TAB	☐
Unannounced		☐
Justification		
By		
Distribution /		
Availability Codes		
Dist	Avail and / or Special	
A-1	20	

14 SUBJECT TERMS

environmental adaptation
freely drifting sensor array
matched-field processing (MFP)
simulated annealing
source localization

15 NUMBER OF PAGES

16 PRICE CODE

17 SECURITY CLASSIFICATION OF REPORT	18 SECURITY CLASSIFICATION OF THIS PAGE	19 SECURITY CLASSIFICATION OF ABSTRACT	20 LIMITATION OF ABSTRACT
UNCLASSIFIED	UNCLASSIFIED	UNCLASSIFIED	SAME AS REPORT

94 1 13 056

UNCLASSIFIED

21a NAME OF RESPONSIBLE INDIVIDUAL	21b TELEPHONE (Include Area Code)	21c OFFICE SYMBOL
G. Chen	(619) 553-4924	Code 732

VLF Source Localization with a Freely Drifting Acoustic Sensor Array

George C. Chen, *Member, IEEE*, and William S. Hodgkiss, *Member, IEEE*

(Invited Paper)

***Abstract*— Source localization and tracking capability of the freely drifting Swallow float volumetric array is demonstrated with matched-field processing (MFP) technique using the 14-Hz cw data collected during the 1989 Swallow float experiment conducted in the northeast Pacific by Marine Physical Laboratory. Initial MFP of the experimental data revealed difficulties in estimating the source depth and range while the source azimuth estimate was quite successful. The main cause of the MFP performance degradation was incomplete knowledge of the environment. An environment adaptation technique using a global optimization algorithm was developed to alleviate the environmental mismatch problem. With limited knowledge of the environment and a known location of the 14-Hz source during a selected time interval according to the source log, the ocean-acoustic environment can be adapted to the acoustic data in a matched-field sense. Using the adapted environment, the 14-Hz source was successfully localized and tracked in azimuth and range within a region of interest using the MFP technique at a later time interval. Two types of environmental parameters were considered, i.e., sound speed and modal wave number. While both approaches yield similar results, the modal wave number adaptation implementation is more computationally efficient.**

***Index Terms*— Matched-field processing, source localization, freely drifting sensor array, environment adaptation, simulated annealing.**

I. Introduction

TRADITIONALLY, source localization has relied on the processing of assumed plane-wave fronts received by spatially distributed sensors to estimate the source bearing or vertical angle of arrivals. In reality, the ocean acoustic channel is extremely complex due to refractive and multipath effects. Assumption of plane-wave arrivals in the processing scheme in some cases can lead to severe degradation of the estimate. Matched-field processing (MFP) has been proposed [1] to actually use the complex ocean acoustic properties to improve source detection and localization. MFP involves the correlation of the actual acoustic pressure field measured at the array with a predicted field due to a source at an assumed location deriving from an acoustic propagation model. A high degree of correlation between the measured field and the predicted field indicates a likely source location. MFP of the acoustic wavefield has shown that when sufficient environmental characterizations (e.g., sound-speed profile, bathymetry, sediment properties) are available, rather remarkable detection and localization results can be obtained. Most available matched-field work has been for rather simple propagation situations (e.g., range-independent environment) and much of the work has been restricted to vertical-line arrays [1]–[9]. Although matched-field processing offers an appealing approach to the underwater source detection and estimation problem, a common difficulty with this technique occurs when the environment information is inaccurate. A "mismatch" occurs between the measured data and the modeled pressure field, and the performance of the MFP is degraded and leads to errors in the estimation of the source location [10]–[14]. Several previous studies such as self-cohering [15], environmentally tolerant beamforming [16], acoustic tomography [17], focalization [18], and MV beamformer with sound-speed perturbation constrains [19] have been proposed to combat the environmental mismatch problem so as to improve the localization performance.

The focus of this paper is twofold: 1) to demonstrate the match-field source localization and tracking capability of the Swallow float freely drifting volumetric array using experimental data, and 2) to propose and demonstrate an environment adaptation technique that may minimize the effect caused by imprecise knowledge of the environment and thereby lead to MFP localization performance enhancement. This paper is organized as follows. Section II gives a brief description of the Swallow float system and a summary of the July 1989 Swallow float experiment. Section III presents the results of initial matched-field processing on the 14-Hz continuous wave (cw) tone collected by the Swallow floats during the 1989 experiment. Controlled simulations also are presented to aid in interpreting the experimental data processing results. Section IV proposes an environment adaptation technique to enhance the MFP localization performance. The technique is illustrated using both simulation and experimental data. Lastly, a summary of the paper is given.

II. 1989 Swallow Float Experiment

A. Swallow Float System Description

Over the last several years, MPL has designed and developed a set of 12 acoustic sensors that are neutrally buoyant and freely drifting when deployed in the ocean. The sensors are called Swallow floats in honor of J. C. Swallow who

Manuscript received January 20, 1993; revised May 7, 1993. This work was supported by the Office of Naval Technology under NRL Contract N00014-88-K-2040.

G. C. Chen is with the Naval Command Control and Ocean Surveillance Center, RDT&E Division, San Diego, CA 92152-5001.

W. S. Hodgkiss is with the Marine Physical Laboratory, Scripps Institution of Oceanography, University of California, San Diego, CA 92152-6400.

IEEE Log Number 9210338.

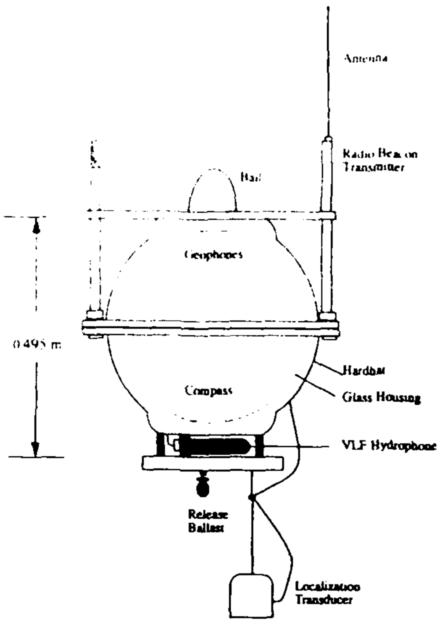

Fig. 1. Schematic drawing of a typical Swallow float.

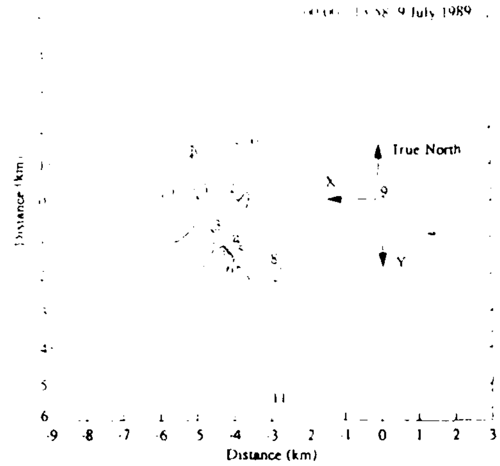

Fig. 2. Float horizontal displacement estimates using least-squares filter during the July 1989 experiment. The circles mark the starting positions.

used freely drifting floats to measure deep ocean currents. The MPL Swallow floats are used to measure acoustic energy in the very low frequency (VLF) band from 1 to 25 Hz. The Swallow floats are designed to operate without tether so that their measurements are not contaminated by tether strumming noise and flow noise. As illustrated in Fig. 1 [20], [21], each Swallow float is a 17-in. diameter glass sphere containing three orthogonally oriented geophones used as the acoustic particle velocity sensor, a compass, the electronics, and power supply. External to the sphere are a hydrophone for measuring VLF acoustic pressure, an 8-kHz acoustic transducer for transmitting and receiving acoustic ranging signals, an optical flash, a radio beacon, and the release ballast. In operation, the floats are deployed and ballasted to neutral buoyancy at the desired depths. While deployed, each float records signals from the three geophones and the hydrophone sampled at 50 Hz, the compass, and the 8-kHz range pulse arrival times. The acoustic transducer with source strength 192 dB re 1 μPa at 1 m generates and receives 8-kHz 10-ms pulses in a programmed sequence. A different float transmits every 45 seconds. When 12 floats are deployed, each float transmits every 9 minutes. The floats are listening whenever they are not transmitting. They receive pulses transmitted by other floats as well as surface/bottom reflections of their own pulses. The interfloat and float-to-surface acoustic travel times can be used to determine the float positions as a function of time with a least-squares-based postprocessing procedure [20].

B. 1989 Experiment Summary

The 12 Swallow floats were deployed for a 24-h period on 8–9 July 1989 near 34°50′N, 122°20′W, about 150 km west-northwest of Pt. Arguello, CA [22]. Of the 12 floats, 9 were freely drifting in the water column, and 3 were tethered to the ocean bottom by 3.05-m lines with 10- to 15-lb anchors. The three bottom-tethered floats were positioned at the corners of a triangle with sides about 6.3 km long in order to provide an absolute reference for the float localization. The nine midwater floats were deployed in a quasi-vertical line array geometry with a vertical float separation of about 400 m, starting at about 600-m depth to about 3800 m. The midwater floats were put into the water at about the geometric center of the bottom-float triangle. Fig. 2 shows the horizontal position estimates of the midwater floats from the least-squares method between 00:00-13:58 PST, 9 July 1989 (records 1003 and 2120). The position estimates indicates that the freely drifting floats dispersed away from the center of the float triangle with floats 0 and 1 (the shallower floats) moving to the northwest, floats 2 and 3 to the west, float 4 to the southwest, and floats 5, 6, 7, and 8 (the deeper floats) to the southeast. The drifting pattern was probably due to the complex water movement near the experiment site. The float depth estimates from the least-squares filter are also plotted in Fig. 3. The estimate of rms float position error is less than 4.6 m [23]. The float localization procedure appeared to be capable of estimating float positions to within the desired accuracy of one-tenth of a wavelength at the highest frequency of interest 25 Hz (6 m) in order to effectively beamform the VLF acoustic data.

As part of a companion experiment, a VLF source was being towed approximately 2500 km west of the Swallow float array at an average speed of 8 knots and depth of 90 m. Fig. 4 shows the VLF source relative to the Swallow float deployment site. The VLF source was to transmit 14 Hz for a half-hour, then 8 Hz for a half-hour, then 14 Hz, then 11 Hz and then repeat the pattern. The power spectral estimates from data collected by float 1's hydrophone during records 1040 to 1680 (00:28-08:28 PST, 9 July 1989) are presented in Fig. 5 in spectrogram format. Evidently, the Swallow floats can see quite clearly the 14-Hz line projected by the VLF source and, at times, the 11-Hz line.

A large volume of environmental data such as AXBT, XBT, and CTD measurements was collected by the companion experiment during 8–10 July 1989 between 34°50′N, 122°20′W

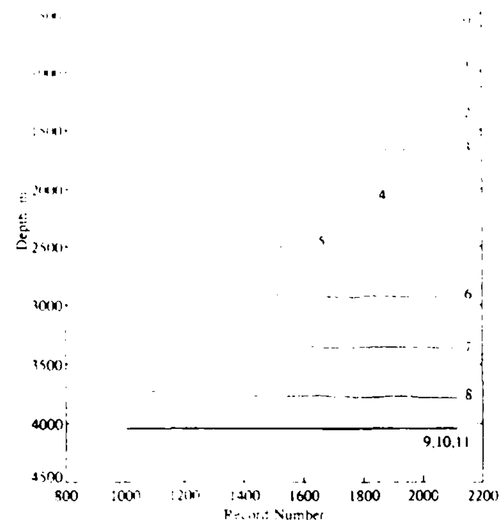

Fig. 3. Float depth estimates using least-squares filter, July 1989 experiment. The horizontal axis of the figure gives the time in units of Swallow float record number. Eighty records represent one hour.

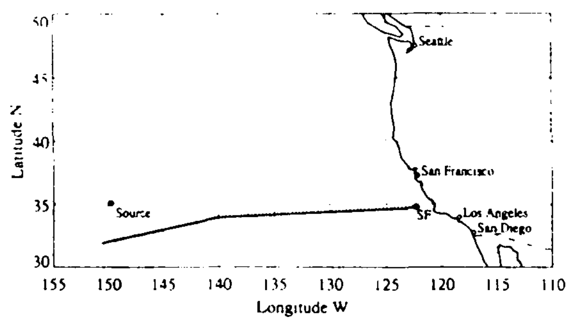

Fig. 4. VLF source—Swallow float array geometry, 9 July 1989. The line of triangles marks the AXBT measurements taken between 8-10 July 1989.

and 32°00′N, 150°00′W. Fig. 6 is the summary of sound speed profiles derived from the measurements.

III. Source Localization With Swallow Float Array

This section presents the results from initial MFP of the 14-Hz-tone propagation collected during the July 1989 Swallow float experiment. There are three steps involved in the MFP. The first step is the estimation of array covariance matrix at the source frequency; the second is the prediction of replica vectors for all assumed source locations; and the last step is the computation of ambiguity surfaces; a peak in the ambiguity surfaces indicates a likely source location. In this study, three array processing structures commonly reported in the literature [7], [24] are used to compute the ambiguity surfaces so that their results can be compared. The Bartlett method is a conventional technique that is robust but ... resolution:

$$P_{\mathrm{Bartlett}}(r, z, \theta) = E^H R E \tag{1}$$

where P is the beamformer output power, E is the replica pressure field vector due to a narrow band source ... θ). R =

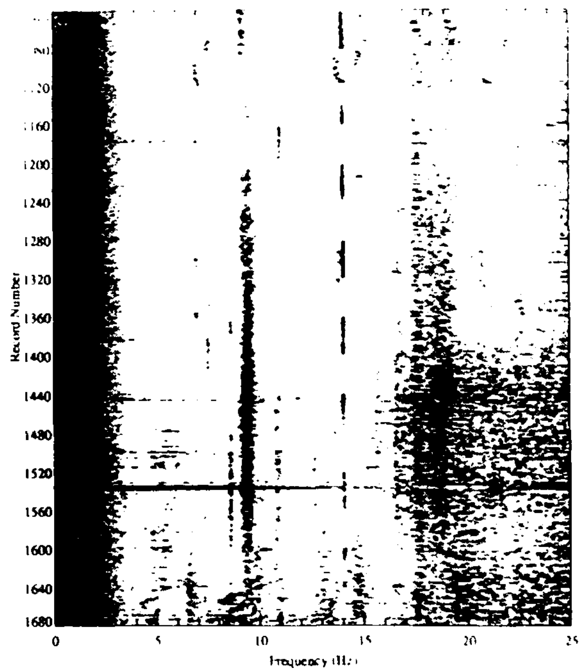

Fig. 5. VLF acoustic spectrogram of float 1, 00:28–08:28 PST, 9 July 1989. The vertical axis of the figure gives the time in units of Swallow float record number. Eighty records represent one hour.

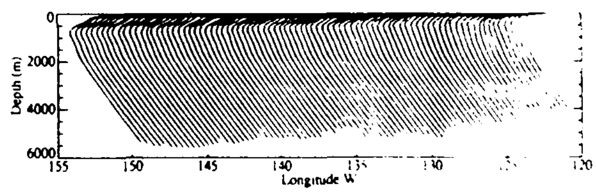

Fig. 6. Sound speed profiles between 150° W and 122° W.

$E[XX^H]$ is the cross-spectral density matrix or array covariance matrix of the sensor outputs, and X is vector of the array Fourier coefficients computed at the frequency of interest. The minimum variance method is a data adaptive technique that yields higher resolution:

$$P_{MV}(r, z, \theta) = \frac{1}{E^H R^{-1} E} \tag{2}$$

and the eigenvector method exploits the orthogonality principal that achieves even higher resolution

$$P_{MUSIC}(r, z, \theta) = \frac{1}{E^H R_N^{-1} E} \tag{3}$$

where R_N is the noise covariance matrix.

A. Estimating the Array Covariance Matrix

Although each Swallow float collects ... channels of geophone data and one channel of hydrophone data, only the omnidirectional hydrophone data from ... drifting floats are studied and analyzed in this paper. ... each float contains its own clock for timing, the first ... processing the acoustic data is to align the time base ... reciprocal path travel times are combined to estimate ... relative clock

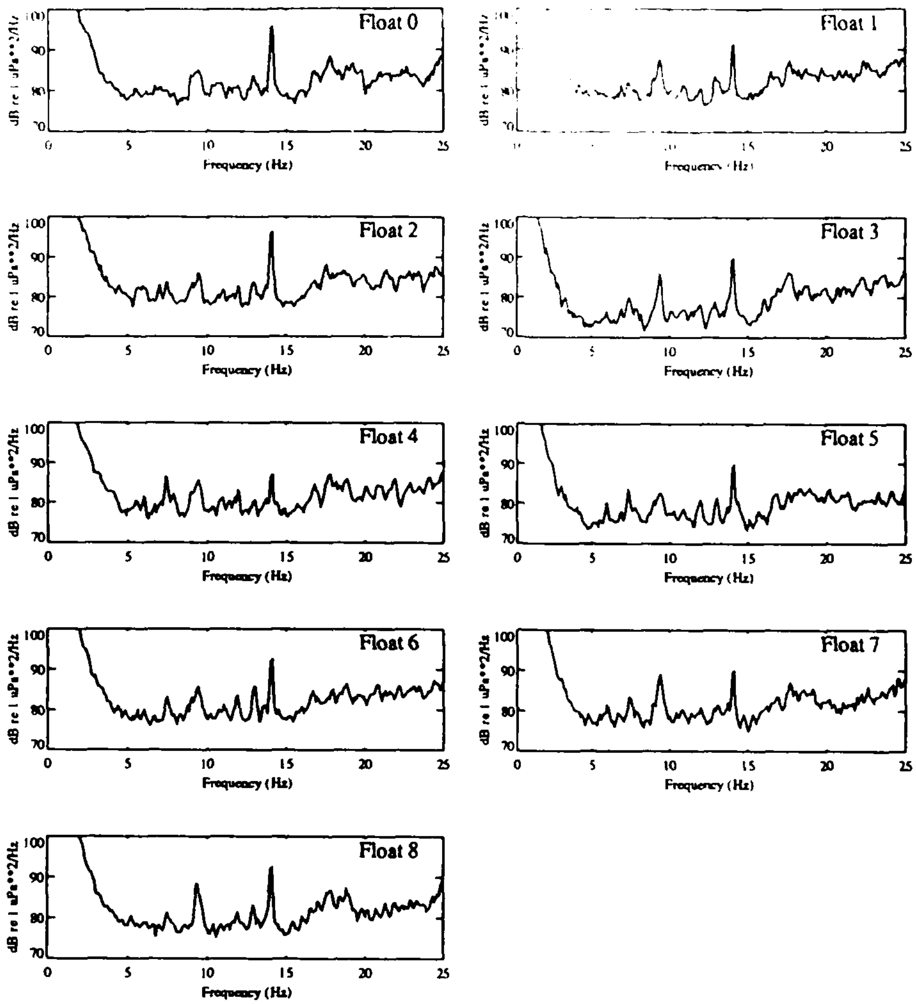

Fig. 7. Acoustic pressure power spectra for midwater floats.

acceleration, clock rate, and the offset between two floats [25]. The time bases are then aligned by choosing one float as a reference whose time base is not shifted and shifting the time base of the rest of the floats' time series. To ensure the quality of the array covariance matrix estimate, the data records need to be qualified and selected with care. Two criteria used in selecting the data record are S/N and spatial coherence at the frequency of interest. Fig. 7 is the power spectra obtained by processing 3 min of data (records 1143 to 1146). The power spectra are derived from incoherently averaging 28, 50% overlapped, 512-point FFTs (97-mHz bin width). A Kaiser-Bessel window with α parameter of 2.5, yielding a sidelobe level of -57 dB [26], weights the data prior to each FFT. Power values are calibrated in decibels re 1 μPa. The 90% confidence level in these spectra is about ± 1 dB. The 14 Hz was being transmitted during the time when data records 1120 through 1160 (01:27–01:57 PST, 9 July 1989) were collected. A line at 14 Hz, about 10 to 15 dB above the background noise, can be clearly seen in all freely drifting floats' pressure spectra. The high S/N at 14 Hz observed in the power spectra illustrates the good quality of the 1989 Swallow float data sets. The second criterion in selecting the data is to estimate the spatial coherence between floats. The spatial coherence or the magnitude-squared coherence (MSC) is defined as

$$|\gamma_{xy}(f)|^2 = \frac{|S_{xy}(f)|^2}{S_{xx}(f)S_{yy}(f)} \tag{4}$$

where $S_{xy}(f)$ is the cross-spectral density at frequency f between $x(t)$ and $y(t)$ with power spectra $S_{xx}(f)$ and $S_{yy}(f)$. The MSC function evaluated at f is a real value, conveniently normalized to lie between zero and unity. High coherence of a line frequency harmonic among all float pairs not only indicates the signals originate from the same source but assures high array gain when the individual sensor outputs are combined to form a beamformer. Fig. 8 shows the magnitude-squared coherence and the phase difference between floats 0 and 2 during 00:27–02:57 PST, 9 July 1989 (records 1040–1240). The MSC functions are calculated by averaging over 40.96 s of data, 128-point FFT's with 50% overlap, providing 31 averages. The high coherence during records 1120 to 1160 is a confirmation that the signal originates from the same source, and the smooth measure of the phase differential suggests that beamforming of this data would be successful.

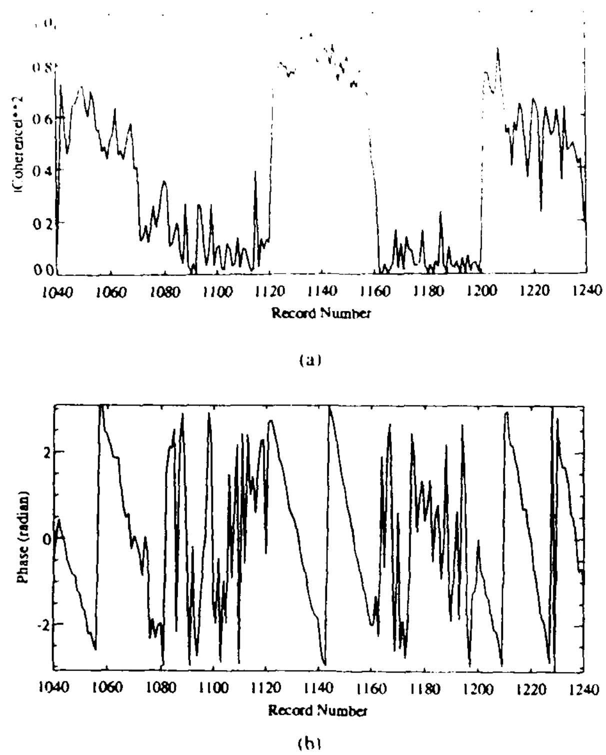

Fig. 8. (a) Spatial coherence at 14 Hz and (b) Phase difference between floats 0 and 2 at 14 Hz during records 1040–1240.

Estimating the array covariance matrix is required by all three processors. The array covariance matrix $\boldsymbol{R}$ can be estimated from the measurement data. Frequency bins of 0.4-Hz width centered at 14 Hz were extracted from 128-point FFT's (2.56 s of data) using a Kaiser–Bessel (with $\alpha = 2.5$) window and 50% overlap for each of the nine floats over a 40.96-s data record. This results in a 31 dyad products $(\boldsymbol{X}\boldsymbol{X}^H)$ being averaged for the covariance matrix estimate. In practice, the number of averages required to produce a reliable covariance matrix estimate is about two to three times the number of sensors in the array. In our case, 31 averages will suffice. Since the matrix must be inverted for the MV processor, it should be well conditioned and of full rank. It is well known that as many dyads as sensors must be averaged to ensure full rank. Although a large number of snapshots (i.e., 31) used to compute the array covariance matrix $\boldsymbol{R}$ ensures the invertibility of the covariance matrix in theory, the condition number of the matrix given by the ratio of the smallest to the largest eigenvalue is below 10^{-6}, and additional effort is required. We use the white-noise stabilization or "diagonal loading" method [27]. The covariance matrix $\boldsymbol{R}$ is stabilized by adding to the main diagonal the quantity 10^{-1} (tr $\boldsymbol{R}/M$) (tr is the trace operator) which corresponds to introducing in the system an uncorrelated sensor noise 10 dB below the average sensor power level [9].

B. Acoustic Propagation Modeling

The second step toward MFP is the calculation of the replica vectors. To predict the acoustic pressure field received by a sensor due to an assumed source, one must model the acoustic environment between the source and the sensor. Fig. 6 is a series of sound speed profiles derived from the CTD's, the XBT's, and the AXBT's taken along the approximate path between the source and the Swallow float array within 48 h of the Swallow float experiment. All of the profiles along the propagation path exhibit a depth excess that is a necessary condition for long range-propagation. The mesoscale change in the ocean temperature structure across range on the order of several thousand kilometers results in range-dependent variations in the sound-speed profile as shown in Fig. 6. The slow varying sound speed structure variation, especially in the upper water column between 120°W and 135°W, is believed to be influenced by the cold waters of the California Current coming down from the north. The sound-speed structure between 140°W and 150°W remains relatively stable; this part of the ocean is known to be environmentally benign.

We use the adiabatic mode theory to model the acoustic pressure field. The adiabatic mode theory solution in a 2-D environment is:

$$p(r, z) = A \sum_{m=1}^{M} u_m(z_o; 0) u_m(z; r) \frac{\exp\left(i \int_0^r \xi_m(s)\, ds\right)}{\sqrt{\xi_m(r) r}}. \tag{5}$$

The modal sum is over the number of propagating modes, M, that exist between the source and the receiver. The modal function involves the depth eigenfunctions at the source $u_m(z_o; 0)$, the receiver $u_m(z; r)$, and the horizontal wave numbers function $\xi_m(s)$ reflecting the range dependence of the medium along the path between the source and the receiver. The implementation strategy for $\int_0^r \xi_m(s)\, ds$ is to divide the full range into a number of segments; the horizontal wave numbers are calculated at a discrete sets of ranges where sound speed measurements are available. To determine the number of propagating modes, M, for the oceanic waveguide formed by the source and the Swallow float array, we need to examine the modal depth eigenfunctions. The modal depth eigenfunctions at a frequency of 14 Hz for the environment near the VLF source and the Swallow float deployment site are computed with the ATLAS normal mode model [28], [29]. The first 30 modal depth eigenfunctions are gray-leveled and displayed in Fig. 9. Examining the upper portion of the figure that corresponds to the environment where the source is located, we see that there are about 22 modes trapped in the water column and are non-bottom interacting; also, for the source depth at 90 m, the first 6 modes are very weakly excited. For the low-order modes to be strongly excited, the source would have to be placed between its turning points where the mode peaks up. The lower portion of the figure corresponds to the environment at the array site; given the water depth at this location, non-bottom interacting modes are limited to the first 16 modes. Note that the depth functions enter [illegible] pressure field calculation in (5) as product $u_m(z_o; 0) u$[illegible] where the one depth function is evaluated at source de[illegible] the other depth function is evaluated at the receiver [illegible]. As result of the product $u_m(z_o; 0) u_m(z; r)$, and ass[illegible] the bottom interacting modes are unable to propagate [illegible] long range due to bottom attenuation, only the first 16 [illegible]

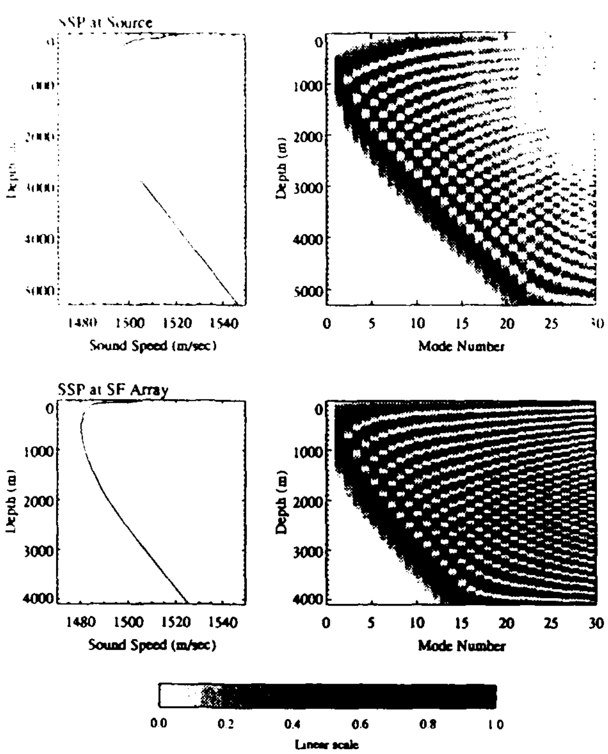

Fig. 9. Modal eigenfunctions at frequency of 14 Hz.

modes were used in the calculation of the acoustic pressure field. Also, in the mode calculation, earth curvature correction was incorporated due to the propagation distance of 2500 km. In this paper, the 3-D replica pressure field was approximated by evaluating the adiabatic model along a series of N bearings in the range-dependent environment assuming the environment is azimuth-invariant, to give an $N \times$ 2-D description of the field [30].

C. Experimental Results

After aligning the float time bases and performing data quality checks, the array covariance matrix for record 1145 (01:47 PST, 9 July 1989) was estimated. The problem of grating lobes in beamforming using a sparse array was not addressed; we therefore limited our focus to a region of interest. The replica vectors were computed using (5) for a hypothetical source in a spatial window extending in range from 2300 km to 2700 km, in depth from 0 to 300 m, and in azimuth from 166° to 176° (refer to Fig. 2, we use the mathematical convention with $-X$ pointing 0° as reference and rotating counterclockwise). The sampling intervals in range, depth, and azimuth were 1000 m, 10 m, and 0.1°, respectively. MFP was performed with all three processors: Bartlett, MV, and MUSIC. The peak value in the region of interest was recorded and normalized to yield power in dB re μPa. Table I summarizes the results of MFP on the experimental data along with the true source location and the expected beamformer output power. Note that power levels were reported for the Bartlett and MV processors only since the MUSIC method does not yield the true power. Fig. 10 present the Bartlett

TABLE I
MFP RESULTS

	Bartlett Processor	MV Processor	MUSIC Processor	[illegible]
Depth of Max	10 m	130 m	10 m	[illegible]
Range of Max	2659 km	2659 km	2659 km	249[illegible] km
Azimuth of Max	172.1°	172.1°	172.1°	171.[illegible]
Power of Max	82.7 dB	73.2 dB	-	87 dB

matched-field ambiguity surfaces. The upper panel was the range-azimuth ambiguity surface evaluated at the depth where the highest peak occurred while the lower panel was the range-depth ambiguity surface evaluated at the azimuth where the highest peak occurred. The surface was normalized to its highest peak and was marked with this symbol, *. For comparison, the true source location was marked with a Δ. While mismatch existed, all three processors were in good agreement except for their depth estimates. In fact, all three lacked the depth resolving power [31]. The highest peak in the ambiguity surface differs from the true location by 0.6° in azimuth and 166 km in range. The large number of sidelobes observed in the ambiguity surfaces was thought to be due to imperfect modeling and the sparseness of the array. The MV and MUSIC processors suffered large losses due to mismatch since the replica were imperfect [31]. Ambiguities (or sidelobes) in range were the result of the repetitive structure of the acoustic field in a convergence zone environment.

D. Controlled Simulation

While source localization in azimuth was somewhat successful, localization in range and depth seemed to be a problem. Simulations are presented here in an effort to understand the experimental ambiguity surfaces. Three simulation cases were studied: the ideal simulation, uncertainty in float positions, and uncertainty in sound speed structure.

1) No Mismatch Simulaton: Assuming there was no mismatch and input S/N was 10 dB, the simulated "acoustic data" and replica vectors were generated using the same environment model. A 14-Hz source was simulated at a range of 2493 km, an azimuth of 171.5°, and a depth of 90 m, which is the true source location at record 1145 according to the source ship log. The Bartlett ambiguity functions were evaluated at a depth of 90 m and an azimuth of 171.5° degrees and plotted in Fig. 11. As expected, the source was correctly localized. The high sidelobes found predominately for the ambiguity surfaces produced by the Bartlett processor were believed to be due to the nature of the processor and the array geometry. Also, the pressure field calculated using the adiabatic normal mode model was composed of only the first 16 low-order waterborne modes. Thus, the acoustic pressure field was less complex or less unique at the simulated source location. The poor depth resolution observed in the ambiguity surfaces was thought to be due to the combination of few propagating modes and the low source depth (90 m) to wavelength (105 m) ratio.

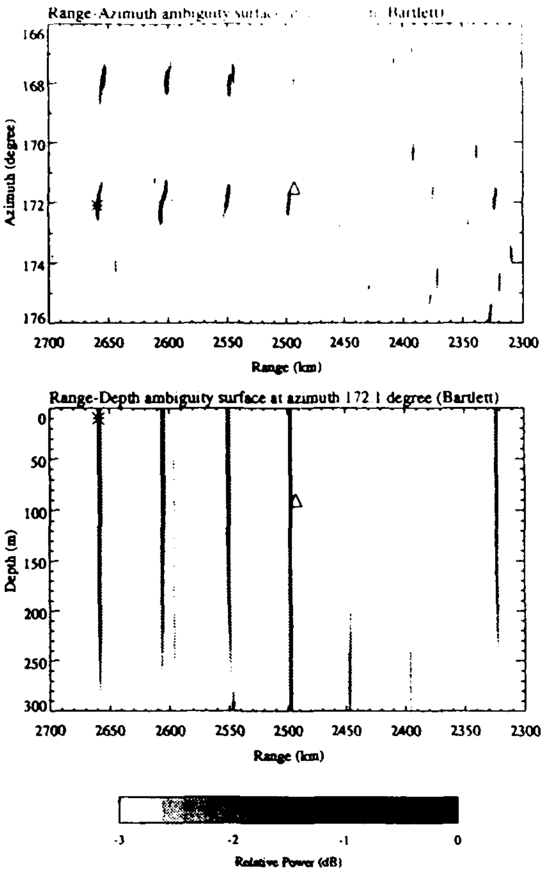

Fig. 10. Matched-field processing results using the Bartlett method for the 14-Hz source during record 1145.

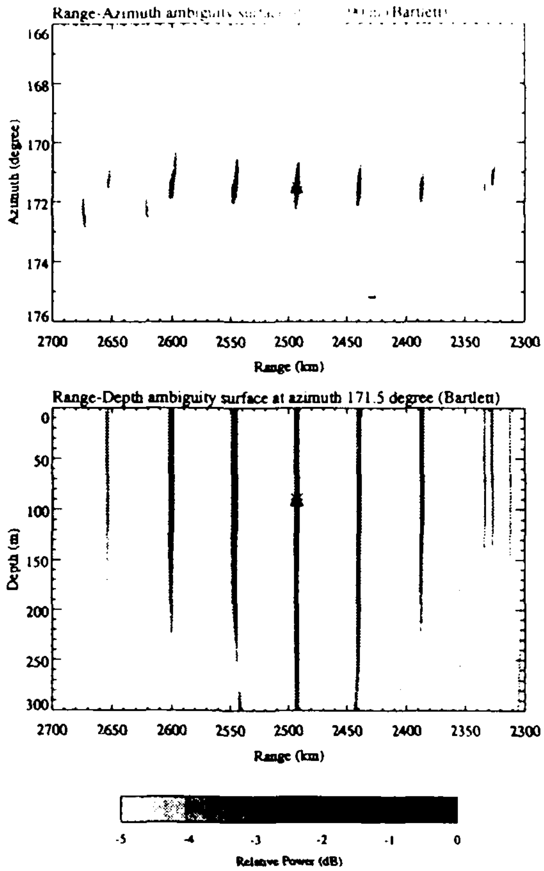

Fig. 11. Matched-field processing simulation results (no mismatch) using the Bartlett method.

2) Uncertainty in Float Positions: The sensitivity to sensor position mismatch was next investigated. Assuming there were no position errors, the replica field were generated using the same conditions as in the real data case. However, the simulated "acoustic data" was computed using a perturbed array geometry where the amount of perturbation to each sensor position had been drawn from a uniform distribution over (4 m, 10 m), similarly the perturbation related to direction had also been drawn from a uniform distribution over $(0, 2\pi)$. The rms position error for the particular realization used in the simulation was 7 m. The impact of mismatch due to float position error was investigated again in a 10-dB input S/N case. The Bartlett range-azimuth ambiguity surface is plotted in Fig. 12(a) and the all three matched field processing results are summarized in Table II.

The sidelobe structures were very similar to those of ideal simulation, but the peak value for the MV and for the MUSIC processor was much reduced from that of the ideal simulation [31]. Although the mismatch reduces the dynamic range of the MV and MUSIC processors tremendously, the source was successfully located in range and azimuth with reduced power. The estimated source range was identical to the "true" source range with a minor discrepancy in the azimuth estimate. These simulated results suggest that slight float position error, i.e., less than one tenth of the wavelength (10.7 m) might be the cause of the mismatch in azimuth but cannot be responsible for the mismatch in range.

3) Uncertainty in Sound-Speed Structure: We then studied the simulation of sound speed mismatch. For simplicity, the sound-speed profiles collected during the experiment were modified by adding a linear function of the form [2]:

$$\Delta c(z) = \frac{\delta(D - z)}{D} \text{ m/s} \tag{6}$$

to the sound-speed profiles collected between 140°W and 150°W. In this simulation, we used $\delta = -3$ and $D = 2000$ m so that at the surface, the sound speed was decreased by 3 m/s, while below 2000 m, there was no change. The specific form (6) is justified for two reasons: 1) The sound-speed profiles collected in this track during the experiment were south of the signal propagation path (refer to Fig. 4) and 2) The general climatic change as one goes from south to north is such that the sound speed in the upper part of the water column decreases. The replica vectors were generated using the original profiles while the simulated "acoustic data" were generated using the modified sound speed profiles reflecting (6). The Bartlett range-azimuth ambiguity surfaces for the sound speed mismatch simulation are plotted in Fig. 12(b) and

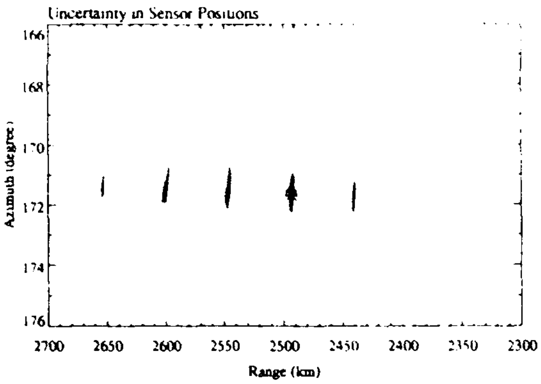

(a)

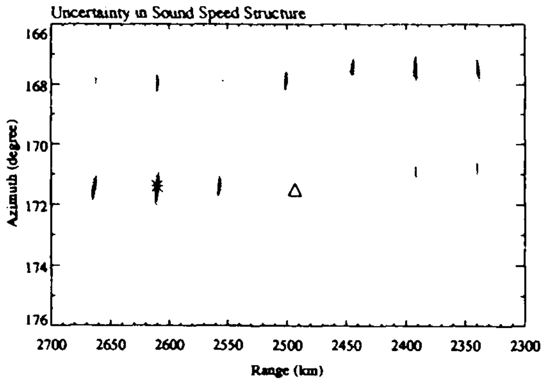

(b)

Fig. 12. Matched-field simulation using the Bartlett Method (a) uncertainty in sensor positions and (b) uncertainty in sound-speed structure.

TABLE II
MATCHED-FIELD SIMULATION OF SENSOR POSITION ERRORS

	Bartlett Processor	MV Processor	MUSIC Processor
Depth of Max.	110 m	110 m	110 m
Range of Max.	2493 km	2493 km	2493 km
Azimuth of Max.	171.7°	171.7°	171.7°
Power of Max.	-0.16 dB	-7.25 dB	–

the MFP results are summarized in Table III. The results show the source peak shifted in range with much reduced power for the MV and MUSIC processors [31]. The estimated source range is off by 117 km from the "true" source range, and the source azimuth is slightly shifted by 0.1°. These simulated results confirmed that uncertainty in sound-speed structures can be responsible for the large mismatch observed in the real-data ambiguity surfaces, particularly the range error. The environmental mismatch problem will be further investigated in Section IV.

IV. Environment Adaptation Matched-Field Processing

MFP has been proposed and developed for localizing underwater acoustic sources by comparing acoustic data with predicted replica pressure fields [1]. The inputs to MFP are the acoustic parameters of the ocean for predicting the replica

TABLE III
MATCHED FIELD SIMULATION OF SO[illegible]

	Bartlett Processor	MV Processor	MUSIC Processor
Depth of Max.	110	110	110
Range of Max.	2610	2610	2610
Azimuth of Max.	171.4°	171.4	171.4
Power of Max.	−0.5 dB	−10.7 dB	

pressure fields and the acoustic data received by an array of hydrophones. In order to compute the replica vectors for the MFP, the knowledge of sound-speed structure and bottom characteristics as a function of depth and range are required. As shown in the previous section, if the available environmental information is not sufficiently accurate, MFP can be degraded even if the signal-to-noise ratio is high. Thus, calibration of the environmental parameters so as to improve the matched-processing performance is of special interest. In this section, we propose an environment adaptation technique which has the potential to enhance the matched-field localization performance. This technique is illustrated using both simulation and experimental data.

A. Environment Adaptation Technique

We envision that the way that the environmental mismatch can be reduced is a two-phase process [15]. 1) Adaptation phase: During this phase, a narrowband signal with frequency of interest at a known location is transmitted to probe the oceanic waveguide. The signal could be a surface ship of opportunity or a broadband source with good S/N at the frequency of interest such as air-deployed shots [17]. The matched-field processor is configured in a feedback loop fashion as in Fig. 13 to adjust the environmental parameters with the goal of causing the predicted pressure field to match the measured pressure field, i.e.,

$$\underset{\Gamma}{\text{maximize}}\ P(r_o, z_o, \theta_o) \tag{7}$$

where Γ is the environmental parameter set, and $P(r_o, z_o, \theta_o)$ is the matched-field processor output power due to source at a known location (r_o, z_o, θ_o). 2) Localization phase: When the environment adaptation phase is completed, the optimized environmental parameter set Γ_{opt} is then used to compute the replica pressure fields and normal matched-field processing can resume to search for an unknown target of interest in the vicinity of the reference source. In this study, two types of environmental parameters, sound-speed structure, and modal horizontal wave number, are considered. We use matched-field processor output as a performance function or cost function, since the cost function P is nonlinear and may have many local maxima (or local minima if we use the negative of P as the cost function); a global optimization technique is required for searching the optimum environmental parameters.

1) Global Optimization Method: In this study, we use the fast annealing method [18], [32] for searching the environmental parameter spaces. The method is based on the conventional simulated annealing technique [33], a heuristic

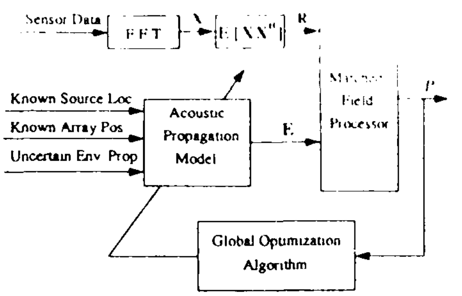

Fig. 13. Environment adaptation technique block diagram.

Monte Carlo search method for the determination of global minimum of combinatorial optimization problems involving many degrees of freedom. Its basic feature is the possibility of exploring the parameter search space of the optimization problem allowing "hill climbing" moves, i.e., the generation of new states (or parameter sets) which increase the cost to allow escape from local minima. These moves are controlled by a dynamic variable called temperature, in analogy with temperature in annealing process. The hill climbing moves are less and less probable as the temperature decreases or cools. Our implementation of the fast simulated annealing algorithm uses the negative of the MUSIC matched-field output power (because of its high resolution capability) as the energy or cost function to be minimized. The fast simulated annealing algorithm for this study is encapsulated in the following procedure.

1) Set the initial temperature T_o to a large value.
2) Determine the number of parameters needed to be perturbed using a random number generator with Poisson distribution and select the parameter to be varied using a random number generator with uniform distribution.
3) Generate the perturbations for the selected parameter(s) using a random number generator with Cauchy distribution [32].
4) Perturb the current parameter set and compute the new cost, E_i, i is the iteration number.
5) If $E_i < E_{i-1}$, then accept the new parameter set and proceed to (7).
6) If $E_i > E_{i-1}$, then accept the new parameters with a probability given by the Boltzmann distribution, $\exp(-\Delta E/kT)$, the quantity k is a constant and its dimension depends on the dimensions of ΔE and T.
7) Decrease the temperature according to the fast cooling schedule [32] which is inversely linear in time, i.e., $T_i = T_o/i$, and repeat the procedure, terminate the procedure when no new parameters are accepted for a large number of interactions.

2) Reducing the Parameter Search Spaces: For combinatorial optimization problems of very many parameters, an efficient characterization to reduce the parameter search space will lead to fast convergence and more uniqueness in the solution [18]. Thus we would like to characterize the environment of interest in as few parameters as possible yet in a meaningful way. A common method from statistics for analyzing data is principal component analysis. The essence of this method is to find a set of K orthogonal vectors in data space that account for as much as possible of the data's variance. Projecting the data from their original N-dimensional space onto the K-dimensional subspace spanned by these vectors then performs a dimensionality reduction that often retains most of the intrinsic information in the data. Typically, $K \ll N$, thus making the reduced data much easier to handle. Similar to the principal component analysis method, oceanographers have developed a method for deriving efficient basis functions, known as empirical orthogonal functions (EOF's), for measured physical quantities such as temperature, salinity, or sound speed as a function of depth [17], [18], [34], [35]. In an effort to reduce the ocean-acoustic parameter spaces, one can describe the parameter set as a sum of EOF's. The EOF's are defined as the eigenvectors $\boldsymbol{V}_i$ of the parameter covariance matrix $\boldsymbol{R}$:

$$\boldsymbol{R}\boldsymbol{V}_i = \lambda_i \boldsymbol{V}_i \tag{8}$$

where λ_i is the ith eigenvalue or the variance associate with $\boldsymbol{V}_i$. The covariance matrix for the environmental data $\boldsymbol{R}$ is defined as

$$\boldsymbol{R} = E[\tilde{\Gamma}\tilde{\Gamma}^T] \tag{9}$$

where $\tilde{\Gamma} = \Gamma - E[\Gamma]$, and Γ is the measured environmental parameter values. $E[\ ]$ is the expectation operator. The parameter search spaces can then be represented or spanned as a linear combination of appropriate EOF's.

$$E[\Gamma] + \sum_{n=1}^{N} \alpha_n \boldsymbol{V}_n \tag{10}$$

where N is the total number of eigenvalues, the $\boldsymbol{V}_n$'s are indexed so that $\lambda_n \geq \lambda_{n+1}$, and α_n's are the EOF coefficients. In practice, a high degree of accuracy can be achieved with only two or three EOF's for representation of ocean-acoustic parameters [17], [35]. Using the EOF approach to parameterize the environment, (7) can now be expressed as

$$\underset{\{\alpha_k,\, k=1,\, K\}}{\text{maximize}} \quad P(r_o, z_o, \theta_o) \tag{11}$$

where $K \ll N$ and α_k is related to Γ by

$$\Gamma = E[\Gamma] + \sum_{k=1}^{K} \alpha_k \boldsymbol{V}_k. \tag{12}$$

B. Simulation Results

The environment adaptation technique described above is first applied to simulation data. To make the simulation as realistic as possible, we modeled the source-array geometry corresponding to the July 1989 experiment with a 14-Hz source deployed at the locations according to the source ship log. The freely drifting sensor array geometries corresponding to the navigation results during the two time intervals, i.e., 01:47 and 04:38 PST, 9 July 1989 were used in the simulation

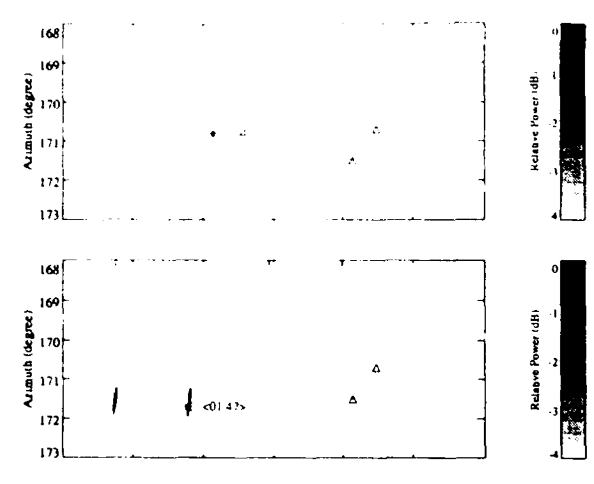

Fig. 14. Matched-field simulation of environmental mismatch for the two time intervals corresponding to the experimental data collected during 1989 experiment.

study. To simulate the environmental mismatch, similar to that of last section, we modified the profiles between 34°N, 140°W and 32°N, 150°W by adding a function of the form:

$$\Delta C(z) = C_{34°\mathrm{N},\,140°\mathrm{W}}(z) - C_{\mathrm{mean}}(z) \text{ m/s} \tag{13}$$

where $C_{34°\mathrm{N},\,140°\mathrm{W}}$ is the sound-speed profile taken at 34°N, 140°W, and C_{mean} is the mean profile between 34°N, 140°W and 32°N, 150°W (refer to the solid line in Fig. 18(b) for the shape of $\Delta C(z)$). Although arbitrary, this perturbation was justified by the fact that the sound-speed profiles collected in this track were off the signal propagation path. The simulated "acoustic data" were generated with an adiabatic normal mode model using the sound speed profiles reflecting (13), while the replica vectors were generated using the original measured sound-speed profiles. The range-azimuth ambiguity surfaces for the mismatched case during the two time intervals are plotted in Fig. 14. The Δ's are the "true" source locations according to the source log, and the *'s are the MFP estimated source locations, i.e., the highest peak in the ambiguity surfaces. As expected, the estimated source locations using the mismatched environment were off in range by roughly 100 km to 150 km (2 to 3 CZ's) for both time intervals.

1) Sound-Speed Adaptation: We now proceed to the environment adaptation technique and assume that the source-array geometry is known exactly during the first time interval (01:47). Under the assumption that the adiabatic approximation is adequate to predict acoustic pressure field in a slowly varying range dependent environment for MFP, one can show that there will be some equivalent range independent sound-speed profile [31]. The first simulation case is to invert for the range-independent sound-speed profile representing the environment along the signal propagation path between 140°W and 150°W in a matched-field sense. Fig. 15(a) shows the excess (demeaned) sound speed profiles for the upper ocean derived from 30 AXBT measurements made between 34°N, 140°W and 32°N, 150°W in July, 1989. Table IV lists the five largest eigenvalues obtained through eigen-decomposition of the sound speed covariance matrix. As can be seen, only the first few eigenvalues are significant. We thus use the eigenvectors or EOF's corresponding to the two largest eigenvalues in spanning the search spaces. Normalized versions of the EOF's corresponding to the two largest eigenvalues are shown as solid and dotted curves, respectively, in Fig. 15(b). The eigenvalues or variances corresponding to these EOF's were $\lambda_1 = \sigma_1^2 = 54.06$ and $\lambda_2 = \sigma_2^2 = 37.96$, respectively. To ensure all possible parameter values are reachable in the search spaces, we allow the values of the EOF coefficients to vary within $\pm 6\sigma_n$. Using the mean sound-speed profile, the first two EOF's, and the initial solution of the EOF coefficients of (0, 0), the optimization is performed with the fast annealing procedure. Fig. 16 shows the convergence properties of a typical annealing run. In this example, the temperature was initialized at 200 and was reduced to 0.2 over 1000 iterations. The first and second panels are the trajectories of the EOF coefficients while the third panel is the cost function learning curve as the annealing proceeds. As expected, the cost function learning curve declines as the iteration goes on, but occasionally the curve increases to a higher energy state thus indicating the escaping out of the local minima. After 350 iterations, the optimization process converges to the minimum energy state, and the solution of the EOF coefficients found at the 1000th iteration is (9.00, 21.91). To validate the optimal solution, the energy (cost function) surface as a function of the EOF coefficient values is calculated exhaustively on a regular grid in α_1 and α_2 (with a grid size of 1) bounded by (−50, 50), which corresponds to 10201 evaluations of the cost function as displayed in Fig. 17. The surface shows a global minimum at $\alpha_1 = 9$, $\alpha_2 = 22$ with numerous local minima scattering around. The joint trajectories of the EOF coefficients as the annealing proceeds are overlaid on the energy surface plot. A good agreement between the solutions obtained by grid search and optimization is observed. It is of interest to know whether the optimal solution of the EOF coefficients varies from run to run. The environment adaptation procedure is then repeated for nine times, each time with 1000 iterations. The solutions are given in Table V. The convergency properties and the consistent agreement among all runs are again observed, which confirms the fitness of the global optimization algorithm.

The adapted sound-speed profile derived from the mean profile and the two EOF coefficients found at the 1000th iteration is plotted by dotted line in Fig. 18. For comparison, the modified sound-speed profiles (i.e., the "true" profiles) used to simulate the "acoustic data" are averaged and plotted by solid line, and the measured profiles that were used to model the replica vectors are averaged and plotted by dashed line. As can be seen, the adapted profile tracks the "true" profile closely. We now proceed to the localization phase of the technique. The measured sound-speed profiles between 140°W and 150°W are replaced by the single adapted sound speed profile, and normal matched-field processing resumes. Fig. 19 shows the optimized range-azimuth ambiguity surfaces for both time intervals. The environmental adapted source locations match those of an ideal simulation (no mismatch).

2) Wave Number Adaptation: The second implementation of the environment adaptation technique is to invert for the modal wave numbers at the source frequency (14 Hz) for

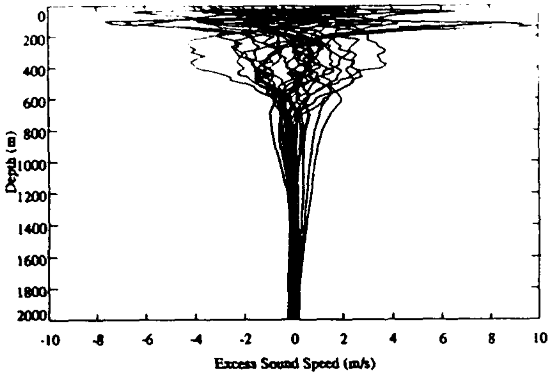

(a)

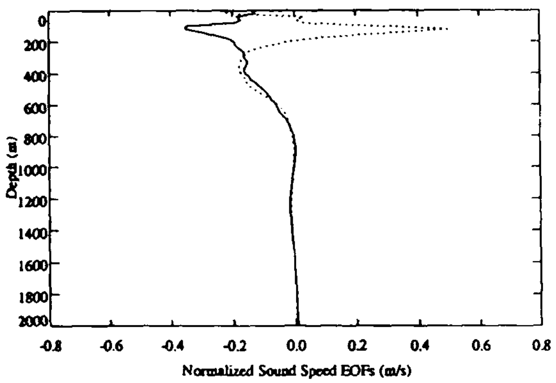

(b)

Fig. 15. (a) Excess (demeaned) sound-speed profiles computed from 30 AXBT measurements made between 140°W and 150°W, July 1989. (b) Normalized versions of the first and second EOF's derived from (a).

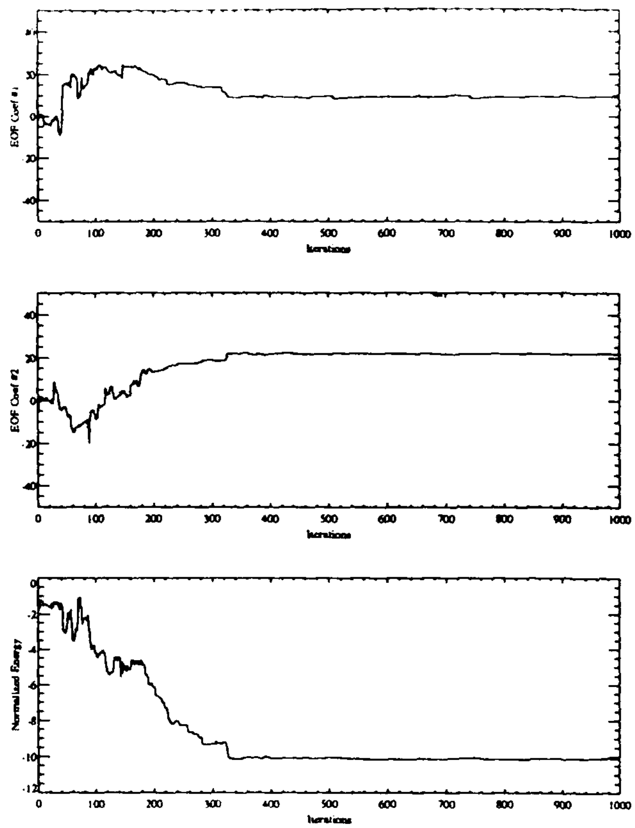

Fig. 16. Trajectories of the sound-speed EOF coefficients and cost function learning curve for a typical annealing run.

TABLE IV
THE FIVE LARGEST EIGENVALUES OBTAINED FROM EIGEN-DECOMPOSITION OF THE SOUND-SPEED COVARIANCE MATRIX

Number	Eigenvalue
1	54.06
2	35.96
3	11.93
4	2.81
5	1.81

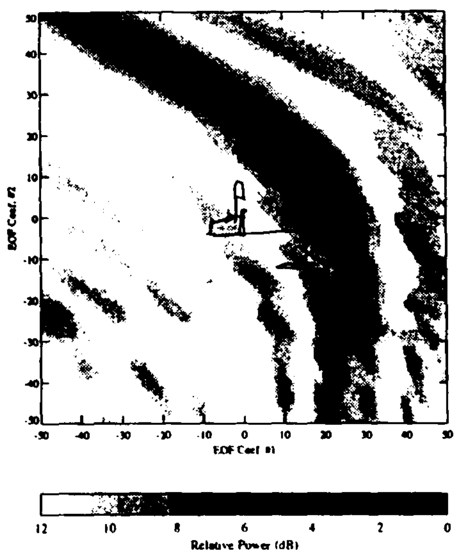

Fig. 17. Energy surface as a function of sound speed EOF coefficients computed by exhaustive search (simulation).

the acoustic waveguide of interest in a matched-field sense. The assumptions and conditions are identical to the sound speed adaptation case with one exception, that is, the modal wave number EOF coefficients are now the search parameters. To compare these two implementations, we followed exactly the same path of investigation. Fig. 20(a) shows the first 16 excess (demeaned) wave number estimates of the modal wave number at the source frequency (14 Hz) obtained from 30 AXBT measurements made in July 1989. Normalized versions of the EOF's corresponding to the two largest eigenvalues are shown as solid and dashed curves in Fig. 20(b). Note that the lag in the wave number covariance matrix estimate is now the mode instead of the depth. Fig. 21 shows the energy surface computed by exhaustive search and an example of the joint trajectories of the wave number EOF coefficients as the annealing proceeds. Using as a reference the averaged model wave numbers derived from the measured profiles, the "true" minus the measured and the adapted minus the measured are plotted by solid and dotted lines, respectively, in Fig. 22. The adapted wave numbers track the "true" wave numbers nicely except for the first five modes. A possible explanation of the

TABLE V
OPTIMIZATION RESULTS FROM NINE RUNS USING SOUND SPEED EOF COEFFICIENTS AS SEARCH PARAMETERS

Run	EOF Coef. #1	EOF Coef. #2
1	9.01	21.88
2	8.96	21.85
3	8.72	22.00
4	8.92	21.89
5	9.09	21.93
6	9.05	21.88
7	9.00	21.97
8	9.05	21.74
9	8.82	22.02

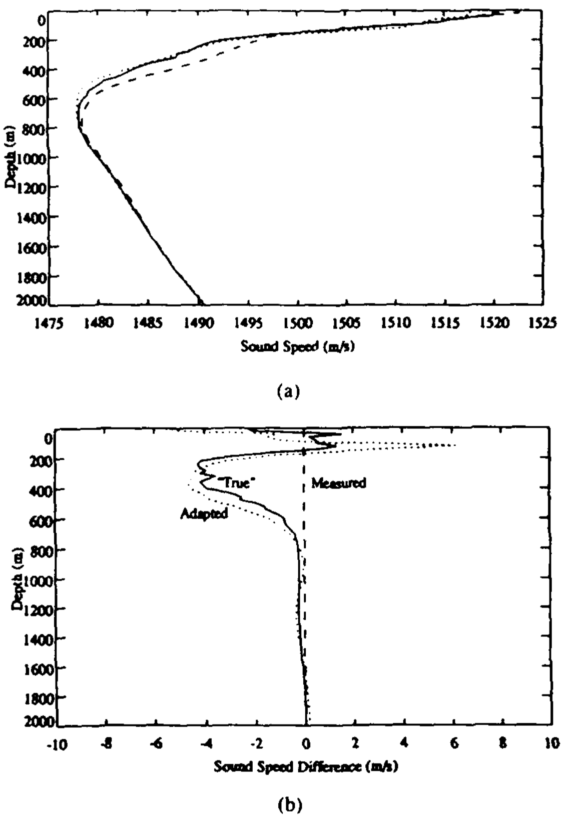

Fig. 18. (a) Sound-speed profile derived from the environment adaptation technique (dotted line), "true" profile (solid line), and measured sound-speed profile (dashed line); (b) the difference version of (a), i.e., using the measured profile as reference (dashed line), the "true" minus the measured and the adapted minus the measured are in solid and dotted lines, respectively (simulation).

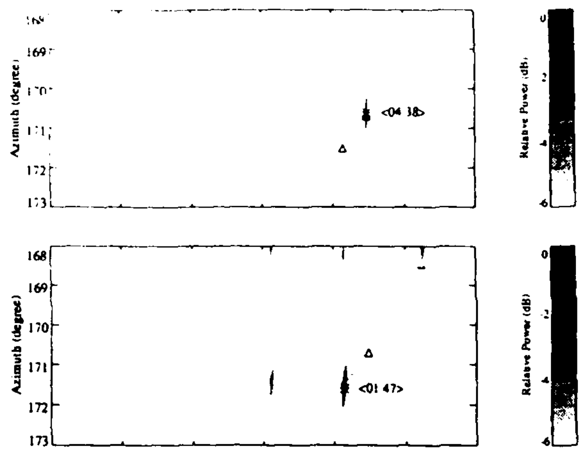

Fig. 19. Self-cohered source locations by environment adaptation technique using sound-speed EOF coefficients as search parameters.

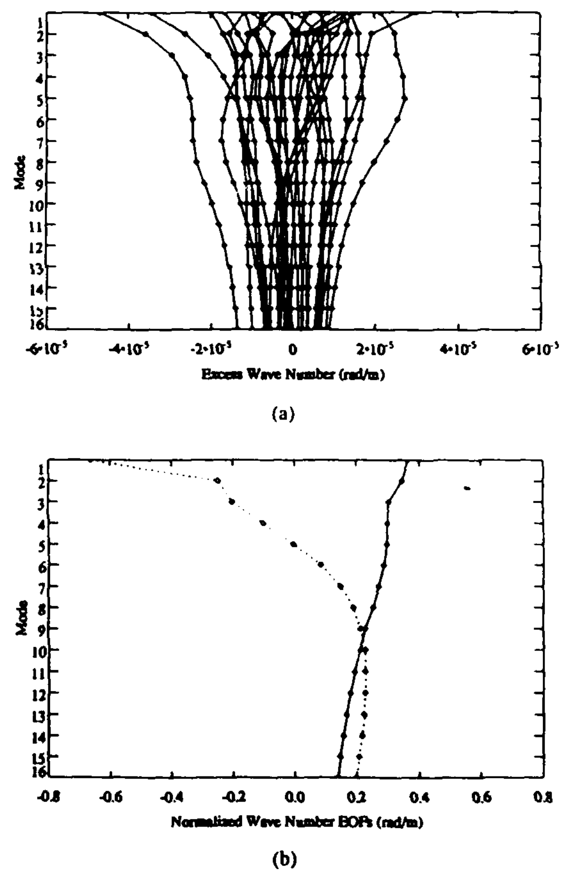

Fig. 20. (a) Excess (demeaned) horizontal wave numbers at 14 Hz derived from 30 AXBT measurements made between 140°W and 150°W, July 1989. (b) Normalized versions of the first and second EOF's derived from (a).

deviation from the "true" wave numbers is that these modes are weakly excited, thus less weight is given during the adaptation process. Again, the environment adapted locations match those of the ideal simulation [31].

It is of interest to know whether the true source location is unique in the neighborhood of the source location. The adaptation procedure is then repeated for each assumed source location within a spatial window extended 16 km in range and 1.5° in azimuth (approximately 60 km in cross range) enclosing the true source location. Fig. 23 confirms that the range-azimuth maximum energy surface indeed has a peak that corresponds to the true source location. This suggests that a weakly range-dependent environment can be approximated by a range-independent environment in a matched-field sense.

Although both implementations of the environment adaptation technique produce similar results under the example given above, the computation burden for the two approaches differs significantly. For the sound speed case, evaluation of the cost function requires the invocation of the acoustic propagation model to compute the modal eigenfunctions and wave numbers

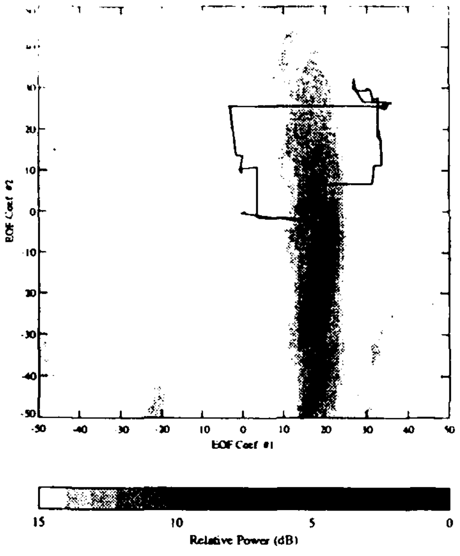

Fig. 21. Energy surface as a function of wave number EOF coefficients computed by exhaustive search (simulation).

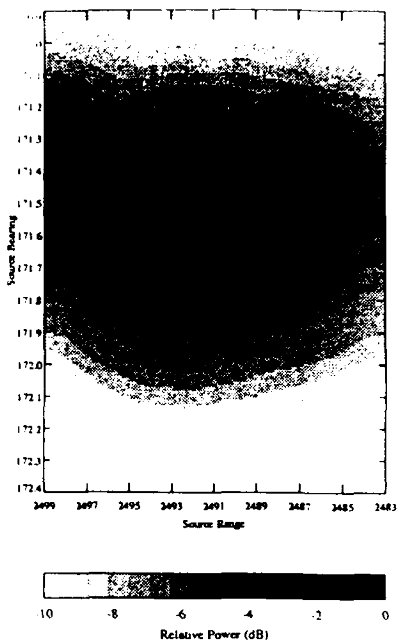

Fig. 23. Range-azimuth energy surface derived from repeating the optimization procedure for each range-azimuth cell (simulation).

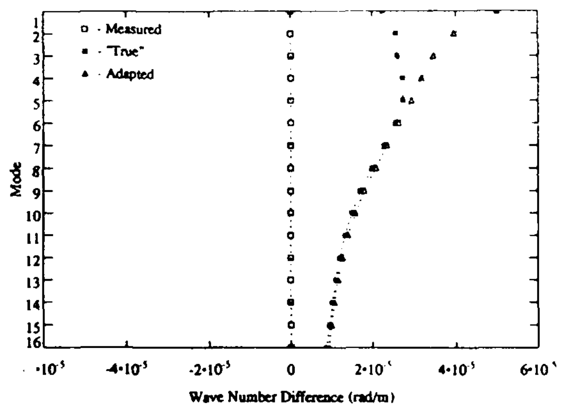

Fig. 22. Deviations in adapted wave numbers and "true" wave numbers from the measured model wave numbers (simulation).

(this is computation intensive). In the wave number adaptation case, the wave numbers are readily available, and updating the wave numbers according to the perturbations involves only a few trivial algebraic steps. The difference in computation performance for the two implementations is at least 3 to 4 orders of magnitude.

C. Experimental Results

Data collected by the Swallow float array during the July 1989 experiment in the northeast Pacific were processed in the same fashion as the simulated data. The acoustic modeling was the same as in the simulation. The data considered here were recorded at 01:47 and 04:38 PST, 9 July 1989. Fig. 24 plots the matched-field range-azimuth ambiguity surfaces for the two intervals with the highest peak marked with *'s and the true source locations marked with Δ's. The shift in the source locations was due to the environmental mismatch as diagnosed through simulation in the last section. We empirically selected the reference source location that corresponded to 01:47 PST, 9 July 1989, by repeating the adaptation procedure for all assumed range-azimuth cells in the neighborhood of the source location obtained from the source log. The highest peak in the range-azimuth maximum energy surface was found at a range of 2489 km and an azimuth 172.1° [31]. We then entered into the adaptation phase of the technique. The sound-speed EOF coefficients were used as search parameters to determine the optimal sound speed structure. Fig. 25 shows the optimized range-azimuth ambiguity surface for both time intervals using the single adapted sound speed structure. As can be seen, the environmental adapted source track mimics the track derived from the source log. The modal wave number adaptation implementation also produced the same results [31]. Table VI lists the adapted source locations versus the source locations according to the VLF source log. The minor discrepancy, a 0.2° to 0.6° shift between the true and adapted source locations, is thought to be due to the slight uncertainty in selecting the coordinate system with respect to true north for the float localization (refer to Fig. 2), since the orientation of the X axis of the coordinate system was taken to be the ship's position when bottomed floats 9 and 10 were put into the water. A relative motion of approximating 60 m in the Y direction between floats 9 and 10 while the floats descended to the bottom would cause the 0.6° rotation in the MFP results. This order of error between ship position and true float position on the bottom has been noted in other Swallow float experiments. In addition, uncertainty in midwater-sensor positions might also contribute to the azimuth error as seen in the simulation study. The minor discrepancy in range error, a 4-km shift, is thought to be due to errors in the assumptions made in modeling the replica vectors. Nonetheless, the relative source movement, a 17-km separation between the two source locations, is found to be consistent with that of the source log.

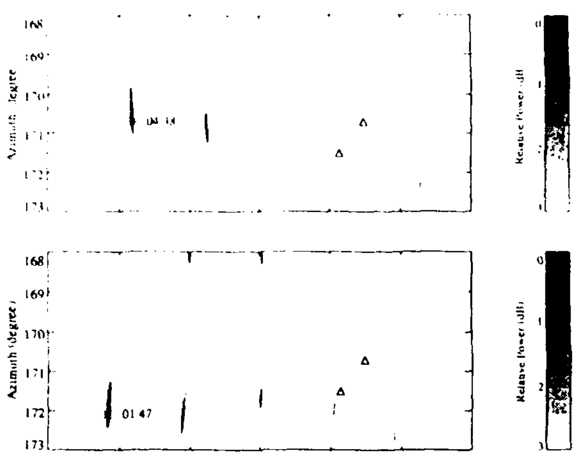

Fig. 24. Matched-field processing of experimental data during the two time intervals.

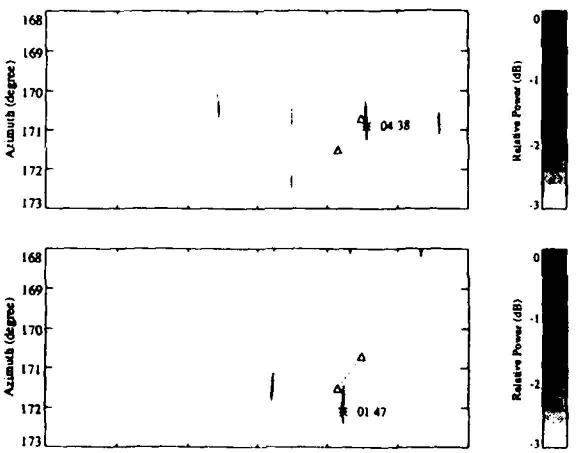

Fig. 25. Self-cohered source locations by environment adaptation technique using sound speed EOF coefficients as the search parameters.

TABLE VI
ENVIRONMENT ADAPTATION MFP RESULTS

Time	True source range	True source azimuth	Adapted source range	Adapted source azimuth
00:47	2493 km	171.5°	2489 km	172.1°
04:38	2476 km	170.7°	2472 km	170.9°

V. CONCLUSIONS

In this paper, we have demonstrated the source localization and tracking capability of a freely drifting volumetric array with MFP using experimental data. We have also proposed and demonstrated an environment adaptation technique to deal with the environmental mismatch problem. Data collected during the 1989 Swallow float experiment were used to perform the study. The geometries of the Swallow float array as a function of time during the 1989 experiment have been estimated using the 8-kHz range measurement with a least-squares based float localization method. The rms position errors estimated by the float localization method is less than 4.5 m, which is within the desired accuracy of one-tenth of a wavelength at the highest frequency of interest 25 Hz (6 m) in order to effectively process the VLF acoustic data coherently. Furthermore, analysis of the experiment acoustic data showed high signal-to-noise ratio and high coherence at 14 Hz among all nine freely drifting floats during some time intervals. The 14 Hz was a continuous wave tonal projected by a VLF source involved in a companion experiment. The high coherence among the floats provided an opportunity for matched-field beamforming of the VLF acoustic data. The replica vectors were modeled with an adiabatic normal mode numerical technique using the environmental data collected during the experiment. Initial MFP of the experimental data experienced difficulties in estimating the source depth and range while the source azimuth estimate was somewhat successful. Controlled simulation using the same conditions as in the real data has revealed that 1) depth resolution indeed is a difficult problem for a shallow VLF source in a long-range environment due to fewer modes being available and due to low source depth-to-wavelength ratio, 2) the range estimate is sensitive to environmental mismatch, and 3) the azimuth estimate is robust. The main cause of the performance degradation has thus been identified to be uncertainty in the environment (i.e., sound-speed mismatch). An environment adaptation technique using a global optimization algorithm was proposed and developed to counteract the MFP performance degradation due to uncertainty in the ocean acoustic environment. We have demonstrated through simulation that with limited *a priori* knowledge of the environment and with a reference source at a known location, the environment can be adapted in a matched-field sense. Using the adapted environment, other unknown source(s) of interest in the vicinity of the reference source can be correctly localized. Applying the environment adaptation technique to experimental data has shown that the 14-Hz source was successfully localized and tracked in azimuth and range within a region of interest using the MFP technique at a later time interval. While both types of environmental parameters, i.e., sound speed and wave number, provided similar results, the modal wave number adaptation implementation has proven to be computationally efficient.

ACKNOWLEDGMENT

The authors are indebted to G. D'Spain and J-M. Tran of the Marine Physical Laboratory for several useful discussions concerning the issues of Swallow float system and random array matched-field processing. They also thank H. Bucker of the Naval Command Control and Ocean Surveillance Center, RDT&E Division, for many useful discussions on the self-cohering technique.

REFERENCES

[1] H. P. Bucker, "Use of calculated sound fields and matched-field detection to locate sound sources in shallow water," *J. Acoust. Soc. Am.*, vol. 59, pp. 368–373, 1976.

[2] M. B. Porter, R. L. Dicus, and R. G. Fizell, "Simulations of matched-field processing in a deep-water Pacific environment," *IEEE J. Ocean Eng.*, vol. OE-12, pp. 173–181, Jan. 1987.

[3] R. G. Fizell, "Application of high-resolution processing to range and depth estimation using ambiguity function methods," *J. Acoust. Soc. Am.*, vol. 82, pp. 606–613, 1987.

[4] A. B. Baggeroer, W. A. Kuperman, and H. Schmidt, "Matched-field processing: Source localization in correlated noise as an optimum parameter estimation problem," *J. Acoust. Soc. Am.*, vol. 83, pp. 571–587, 1988.
[5] J. M. Ozard, "Matched-field processing in shallow water for range, depth, and bearing determination: Results of experiment and simulation," *J. Acoust. Soc. Am.*, vol. 86, pp. 744–753, Aug. 1989.
[6] C. Feuillade, W. A. Kinney, and D. R. Del Balzo, "Shallow-water matched-field localization off Panama City, Florida," *J. Acoust. Soc. Am.*, vol. 88, pp. 423–433, July 1990.
[7] C. Z. Zala and J. M. Ozard, "Matched-field processing in a range-dependent environment," *J. Acoust. Soc. Am.*, vol. 88, pp. 1011–1019, Aug. 1990.
[8] B. J. Sotirin, J-M. Q. D. Tran, and W. S. Hodgkiss, "Matched-field processing of deep-water ambient noise," *IEEE J. Oceanic Eng.*, vol. OE-15, pp. 316–323, Oct. 1990.
[9] J-M. Q. D. Tran, and W. S. Hodgkiss, "Matched-field processing of 200 Hz continuous wave (cw) signals," *J. Acoust. Soc. Am.*, vol. 89, pp. 745–755, Feb. 1991.
[10] A. Tolstoy, "Sensitivity of matched-field processing to sound speed profile mismatch for vertical arrays in a deep water Pacific environment," *J. Acoust. Soc. Am.*, vol. 85, June 1989.
[11] C. Feuillade, D. R. Del Balzo, and M. M. Rowe, "Environmental mismatch in shallow water matched-field processing: Geoacoustic parameter variability," *J. Acoust. Soc. Am.*, vol. 85, June 1989.
[12] R. M. Hamson and R. M. Heitmeyer, "Environmental and system effects on source localization in a shallow water by the matched-field processing of a vertical array," *J. Acoust. Soc. Am.*, vol. 86, pp. 1950–1959, Nov. 1989.
[13] D. F. Gingras, "Methods for predicting the sensitivity of matched-field processors to mismatch," *J. Acoust. Soc. Am.*, vol. 86, pp. 1940–1949, Nov. 1989.
[14] J. R. Daugherty and J. F. Lynch, "Surface wave, internal wave, and source motion effects on matched-field processing in a shallow water waveguide," *J. Acoust. Soc. Am.*, vol. 87, pp. 2503–2526, June 1990.
[15] H. P. Bucker, "Self-coherent matched-field processing," *Fourth Matched-Field Processing Workshop, Defence Research Establishment Pacific*, Sept. 1989.
[16] H. Schmidt, A. B. Baggeroer, W. A. Kuperman, and E. K. Sheer, "Environmentally tolerant beamforming for high-resolution matched-field processing: Deterministic mismatch," *J. Acoust. Soc. Am.*, vol. 88, pp. 1802–1810, 1990.
[17] A. Tolstoy, O. Diachok, and L. N. Frazer, "Acoustic tomography via matched-field processing," *J. Acoust. Soc. Am.*, vol. 89, pp. 1119–1127, Mar. 1991.
[18] M. D. Collins and W. A. Kuperman, "Focalization: environmental focusing and source localization," *J. Acoust. Soc. Am.*, vol. 90, pp. 1410–1422, Sept. 1991.
[19] J. K. Krolik, "Match-field minimum variance beamforming in a random ocean channel," *J. Acoust. Soc. Am.*, vol. 92, pp. 1408–1419, Sept. 1992.
[20] R. L. Culver and W. S. Hodgkiss, "Comparison of Kalman and least squares filters for locating autonomous very low frequency acoustic sensors," *IEEE J. Oceanic Eng.*, vol. OE-13, pp. 282–290, 1988.
[21] G. L. D'Spain, W. S. Hodgkiss, and G. L. Edmonds, "The simultaneous measurement of infrasonic acoustic particle velocity and acoustic pressure in the ocean by freely drifting Swallow floats," *IEEE J. Oceanic Eng.*, vol. 16, pp. 195–207, Apr. 1991.
[22] G. C. Chen, G. L. D'Spain, W. S. Hodgkiss, and G. L. Edmonds, "Freely drifting Swallow float array: July 1989 trip report," *MPL TM-420*, Marine Physical Laboratory, Scripps Institution of Oceanography, San Diego, CA, 1990.
[23] G. C. Chen and W. S. Hodgkiss, "Localizing Swallow floats during the July 1989 experiment," *MPL TM-421*, Marine Physical Laboratory, Scripps Institution of Oceanography, San Diego, CA, 1990.
[24] D. H. Johnson, "The application of spectral estimation methods to bearing estimation problems," *Proc. IEEE*, vol. 70, pp. 1018–1028, Sept. 1982.
[25] R. L. Culver, G. L. D'Spain, W. S. Hodgkiss, and G. L. Edmonds, "Estimating 8 kHz pulse travel times and travel times error from Swallow float localization system measurements," Unpublished Notes, Marine Physical Laboratory, Scripps Institution of Oceanography, San Diego, CA, 1989.
[26] F. J. Harris, "On the use of Windows for harmonic analysis with the discrete Fourier-transform," *Proc. IEEE*, vol. 66, pp. 51–83, 1978.
[27] B. D. Carlson, "Covariance matrix estimation errors and diagonal loading in adaptive arrays," *IEEE Trans. Aerosp. Electron. Syst.*, vol. 24, pp. 397–401, 1988.
[28] D. F. Gordon and H. P. Bucker, "Arctic acoustic propagation model with ice scattering," *NOSC Tech. Rep. 985*, Naval Ocean Systems Center, San Diego, CA, 30 Sept. 1984.
[29] F. Ryan, "ATLAS Normal Mode Model," Version 2.19., Naval Ocean Systems Center, San Diego, CA.
[30] J. S. Perkins and R. N. Baer, "An approximation to the three-dimensional parabolic-equation method for acoustic propagation," *J. Acoustic Soc. Am.*, vol. 72, pp. 515–522, Aug. 1982.
[31] G. C. Chen, "VLF source localization with a freely-drifting sensor array," MPL-U-45/92, Marine Physical Laboratory, Scripps Institution of Oceanography, San Diego, CA, 1992.
[32] H. Szu and R. Hartley, "Fast simulated annealing," *Phys. Lett. A*, vol. 122, pp. 157–162, June 1987.
[33] S. Kirkpatrick, C. D. Gellat, and M. P. Vecchi, "Optimization by simulated annealing," *Science*, vol. 220, pp. 671–680, May 1983.
[34] E. R. Davis, "Predictability of sea surface temperature and sea level pressure anomalies over the North Pacific Ocean," *J. Phys. Ocean.*, pp. 249–266, May 1976.
[35] L. R. LeBlanc and F. H. Middleton, "An underwater acoustic sound velocity data model," *J. Acoust. Soc. Am.*, vol. 67, pp. 2055–2062, June 1980.

George C. Chen (M'89) received the M.S. degree in computer science from the University of California at Los Angeles in 1981 and the Ph.D. degree in electrical engineering from the University of California at San Diego in 1992.

Prior to 1985, he was a software engineer with the Computer Sciences Corporation, El Segundo, CA, and worked on computer networking and database systems. Since 1985 he has been a research engineer with the Naval Command, Control and Ocean Surveillance Center's RDT&E Division (formally Naval Ocean Systems Center), San Diego, CA. His research interests include digital signal processing, communication systems, and neural networks.

William S. Hodgkiss (S'68–M'75) received the B.S.E.E. degree from Bucknell University, Lewisburg, PA, in 1972, and the M.S. and Ph.D. degrees from Duke University, Durham, NC, in 1973 and 1975, respectively.

From 1975 to 1977 he worked with the Naval Ocean Systems Center, San Diego, CA. From 1977 to 1978 he was a faculty member in the Electrical Engineering Department, Bucknell University, Lewisburg, PA. Since 1978 he has been a member of the faculty of the Scripps Institution of Oceanography and on the staff of the Marine Physical Laboratory, University of California, San Diego. He is the Applied Ocean Science curricular group coordinator, Graduate Department of the Scripps Institution of Oceanography. His present research interests are in the areas of adaptive digital signal processing, adaptive array processing, applications of these to underwater acoustics, the propagation of acoustic energy in the ocean and its interaction with the sediments beneath the ocean and the sea surface, and the statistical properties of ambient ocean noise.